Nano Energy 143 (2025) 111318

Contents lists available at ScienceDirect

Nano Energy

journal homepage: www.elsevier.com/locate/nanoen

A ternary-dielectric rolling TENG array for robust ocean energy harvesting and distributed environmental monitoring

Ziyue Xi [a,1], Hengxu Du [a,1], Yawei Wang [b,1], Hongyong Yu [a], Shu Dai [c], Mingli Fan [a], Jingyi Liu [a], Quanke Su [d], Hao Wang [a,*], Guobiao Hu [b,*], Minyi Xu [a,*]

[a] Dalian Key Lab of Marine Micro/Nano Energy and Self-powered System, Dalian Maritime University, Dalian, Liaoning 116026, China
[b] Thrust of Internet of Things, The Hong Kong University of Science and Technology (Guangzhou), Nansha, Guangzhou 511400, China
[c] Shanghai Investigation, Design & Research Institute Co., Ltd., Shanghai 200335, China
[d] Thrust of Intelligent Transportation, The Hong Kong University of Science and Technology (Guangzhou), Nansha, Guangzhou 511400, China

ARTICLE INFO

Keywords:
Triboelectric nanogenerator
Rolling-mode design
Buoy array
Distributed sensing
Wireless ocean sensing

ABSTRACT

Wave energy is a promising renewable energy source for marine applications. However, its low frequency and variability pose challenges for efficient energy conversion. This study presents a novel rolling-mode triboelectric nanogenerator (R-TENG) designed for self-powered wireless ocean monitoring. Configured as an array, the system can not only enhance spatial coverage and energy robustness but also enable distributed sensing. To guide the design, hydrodynamic simulations using WAMIT were carried out to evaluate the buoy's dynamic response in the frequency domain. The output of the R-TENG was further boosted using an integrated power modulation strategy. Experimental results showed that a four-unit R-TENG array could charge a 10,000 μF up to 5 V in 175 s at a low frequency of 0.1 Hz and achieve a peak power of 114.3 mW with an optimal load of 5 MΩ. A wireless ocean sensing system was developed, supporting real-time monitoring of pH and temperature. Both forced motion experiments and nearshore sea trials validated the functionality of the integrated system, from energy harvesting and sensing to wireless data transmission to an onshore receiver. This work demonstrates a scalable and durable solution for self-sustained, distributed marine environment monitoring, paving the way for sustainable maritime Internet of Things.

1. Introduction

Wave energy is a clean and renewable ocean energy source, with a global reserve estimated to be trillions of kilowatts [1]. Compared to other forms of ocean energy, such as tidal, current, and temperature difference energy, wave energy offers extensive distribution, good spatial and temporal predictability, and relatively high energy density. These characteristics make wave energy particularly well-suited for powering floating buoys and other small-scale marine monitoring devices through innovative designs [2,3]. Triboelectric nanogenerators (TENGs), as a novel technology for harvesting high-entropy wave energy, provide advantages in direct conversion and environmental adaptability, which can be used to develop cost-effective wave energy harvesters [4–6].

In recent years, various innovative approaches have been proposed to improve the energy harvesting performance of TENGs, including float-based models [7], turntable configurations [8–10], rolling mode systems [11–14], bionic-inspired structures [15,16], liquid-solid mode designs [17,18], as well as optimizations conducted in mechanical structures [19–21] and materials [22,23]. Despite the great potential of TENGs, they still face numerous challenges in practical applications. For example, the power outputs from TENGs under lower frequency or lower amplitude wave excitations in real ocean conditions are limited in powering marine equipment [24]. The low friction and smooth movement of the balls in rolling TENGs contribute to good startup characteristics, enabling them to operate effectively even under low-amplitude motion [25,26]. A grating electrode configuration helps reduce the internal resistance of TENGs and improves current output by facilitating charge transfer [27]. The integration of the rolling mode with the grating electrode design greatly enhances the wave energy harvesting performance of TENGs [28]. However, the energy harvesting capacity of a single TENG unit still remains limited.

* Corresponding authors.
E-mail addresses: hao8901@dlmu.edu.cn (H. Wang), guobiaohu@hkust-gz.edu.cn (G. Hu), xuminyi@dlmu.edu.cn (M. Xu).
[1] These authors contribute equally to this work.

https://doi.org/10.1016/j.nanoen.2025.111318
Received 17 May 2025; Received in revised form 1 July 2025; Accepted 10 July 2025
Available online 11 July 2025

Constructing a TENG array provides a way to enhance the overall wave energy harvesting capability. A distributed buoy array can cover a broader ocean area, mitigate the energy shortfall impact due to local energy fluctuations, and strengthen the overall operational robustness [29]. Moreover, compared to a single TENG-powered buoy that can monitor only one location, a buoy array can form a distributed sensing network capable of capturing and reconstructing the spatial distribution characteristics of ocean parameters [30,31]. In addition, these arrays can be equipped with various sensors (e.g., pH, temperature) to enable multi-dimensional monitoring of the marine environment, thereby broadening their applications in ocean sensing and environmental assessment.

Extensive studies have been conducted on array designs to improve both energy conversion efficiency and sensing capabilities [32–35]. For instance, Liu *et al.* [36] proposed a 6 × 4 cross-vertical double-layer electrode array device that facilitates wave prediction. Ouyang *et al.* [37] designed a TENG array based on a copper particle-PTFE tube structure with a power amplification ability. Duan *et al.* [38] developed a three-dimensional rolling ball TENG array for large-scale ocean energy harvesting. In general, scaling up wave energy harvesting through arrays has become a popular trend in future development.

In this work, a buoy array based on a rolling-mode triboelectric nanogenerator (R-TENG) is proposed. The R-TENG primarily comprises a PLA shell, rolling PTFE balls, nylon balls, and grating electrodes. The track-type shell combined with rolling balls enhances the startup capability of the R-TENG, while grating electrodes effectively reduce the internal resistance. The use of a ternary dielectric composed of PTFE, nylon, and copper further improves the TENG's output performance. Arranging R-TENGs in an array enables wave energy harvesting over a broader area. Additionally, different buoys can be equipped with various sensors to collect more comprehensive ocean data, such as temperature and pH, as in this study.

The buoy's motion was first analyzed and predicted using WAMIT, a widely recognized frequency domain hydrodynamic analysis software. In addition, a power modulation strategy was employed to enhance the charging capability of the R-TENG buoy array in practical applications. Notably, in the forced motion experiments, the four-unit R-TENG buoy array delivered a peak power of 114.3 mW and successfully powered 150 LED bulbs. Sea trials further examined its ability to support wireless sensing of temperature and pH levels. These results demonstrated the TENG array's improved energy harvesting performance, expanded sensing capabilities, and potential as a robust solution in marine IoT.

2. Results and discussions

2.1. Fundamental working mechanism

Fig. 1a illustrates the application scenario of the R-TENG array. Subjected to wave-induced oscillatory motion, the R-TENG unit inside each buoy can convert wave energy into electricity, enabling in-situ power generation for wireless sensor nodes and supporting real-time data transmission. Moreover, the array configuration expands the geographic coverage and supports the spatially resolved monitoring of oceanographic data.

Fig. 1b presents the detailed structural design of the buoy, which consists of an outer shell, an internal frame, a power generation module, and a counterweight. The power generation unit comprises a PLA track shell, PLA baffles, grid-patterned copper electrodes, PTFE balls, and nylon balls. The track-type shell design reduces the friction during ball movement, facilitating operation under low-amplitude wave conditions, improving durability and enhancing the effective motion of the balls. Copper foil is affixed to the shell in a grating electrode layout to lower

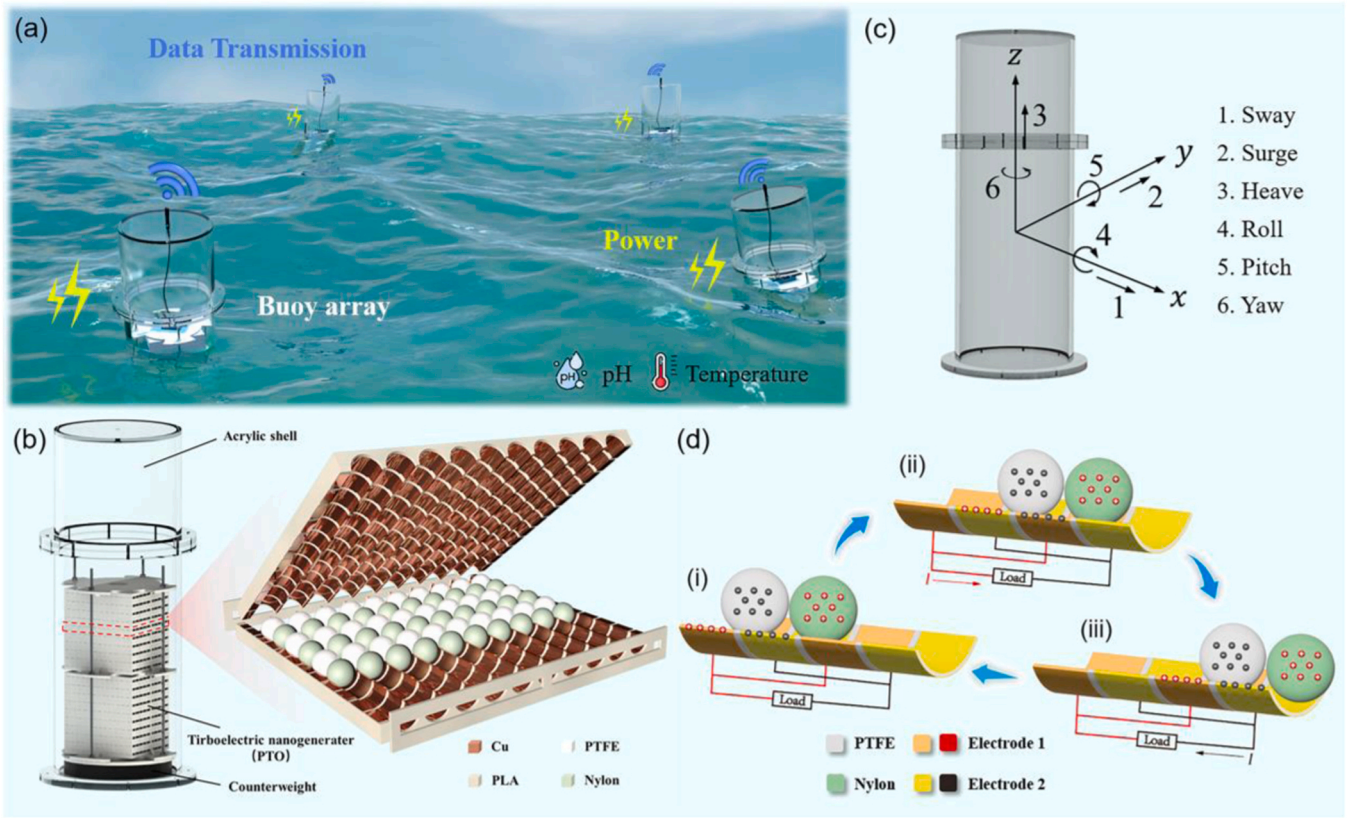

Fig. 1. Application scenario, structural design, and working principle of the R-TENG array. (a) Application of the R-TENG array for distributed ocean sensing and wireless data transmission. (b) Structural design of the buoy and internal configuration of the R-TENG. (c) Illustration of the six degrees of freedom in buoy motion (d) Working mechanism of the R-TENG based on the rolling motion of dielectric balls within the internal track.

the internal resistance and increase the capacitance between electrodes, thereby enhancing electrostatic induction and boosting the current output of the R-TENG.

Two types of balls, i.e., PTFE and nylon balls, with opposite triboelectric polarities, are combined with the copper electrode to form a ternary dielectric structure, thereby enhancing charge generation and transfer. As the three materials yield different charge affinities, electrons migrate from high-energy orbitals to low-energy vacant states upon contact until potential well equilibrium is achieved. Fig. S1 depicts the electron cloud potential well model for this ternary dielectric design, illustrating the charge transfer mechanism behind the three dielectric materials during surface contact [39].

Based on the design of the R-TENG unit, the motion of the buoy carrying the R-TENG is also important. A floating buoy typically exhibits motion in six degrees of freedom, including heave, surge, sway, pitch, yaw, and roll, as shown in Fig. 1c. The R-TENG design is well-suited for near-shore wave conditions, primarily harnessing energy from pitch motion. To predict the buoy's motion characteristics in waves, a hydrodynamic analysis is first conducted. Based on the potential flow theory, the buoy's hydrodynamic behavior is assessed. The six DOF motion amplitudes of a body ξ_j can be computed by solving a 6×6 linear system [40]:

$$\sum_{j=1}^{6} \left[-\omega^2 \left(M_{ij} + A_{ij}\right) + iwB_{ij} + C_{ij} \right] \xi_j = Xi \tag{1}$$

where ξ_j ($j = 1, 2, \ldots, 6$) is the complex amplitude of the body motion in the j-th degree-of-freedom (DOF), M_{ij} is the 6×6 mass matrix, A_{ij} is the 6×6 added mass matrix, B_{ij} is the 6×6 radiation damping matrix, C_{ij} is the 6×6 hydrostatic stiffness matrix, X_i represents the complex wave excitation forces. The mass matrix M_{ij} can be expressed as:

$$M = \begin{pmatrix} m & 0 & 0 & 0 & mz_g & -my_g \\ 0 & m & 0 & -mz_g & 0 & mx_g \\ 0 & 0 & m & my_g & -mx_g & 0 \\ 0 & -mz_g & my_g & I_{11} & I_{12} & I_{13} \\ mz_g & 0 & -mx_g & I_{21} & I_{22} & I_{23} \\ -my_g & mx_g & 0 & I_{31} & I_{32} & I_{33} \end{pmatrix} \tag{2}$$

where m is the body mass and (x_g, y_g, z_g) are the center of gravity coordinates. The moments of inertia I_{ij} are defined in terms of the corresponding radii of gyration r_{ij} as follows:

$$I_{ij} = \rho V r_{ij} \left| r_{ij} \right| \tag{3}$$

where ρ is the water density, and V is the submerged volume. For the buoy, as both the volume distribution and the mass distribution are designed to be approximately symmetric with x-axis and y-axis, very small coupling between roll and pitch will be expected.

The R-TENG operates in the rolling freestanding layer mode, its output performance under different states can be explained by the following equation [41]:

$$J_{SC} = \frac{d\Delta\sigma_{SC}}{dt} \tag{4}$$

where J_{SC} is the short circuit charge density, σ_{SC} is the surface charge density, t is the time. As the wave frequency and pitch amplitude increase, the speed of the balls inside the R-TENG increases, which in turn reduce the dt term in Eq. (4). Therefore, the output of the R-TENG will increase.

Fig. 1d further illustrates the power generation process of the proposed TENG. The R-TENG design uses grating electrodes, with orange and yellow representing Electrode 1 and Electrode 2, respectively. Taking Fig. 1d(i) as the initial state, the charge affinity of the three materials follows the order PTFE>Cu>Nylon, ensuring that the charge transfer occurs between PTFE and Nylon via the copper electrode. In this initial state, the PTFE balls and nylon balls carry equal amounts of negative and positive charges. When subjected to wave excitation, the PTFE and nylon balls roll between grating copper electrodes. As they reach the position shown in Fig. 1d(ii), electrons are transferred through the grating electrodes via an external circuit, thus generating an induced current. When the balls continue rolling to the position in Fig. 1d(iii), an induced current in the opposite direction is generated.

2.2. Buoy hydrodynamic analysis

Based on the above theoretical framework, the response amplitude operator (RAO) of the floating TENG buoy is analyzed using WAMIT, a well-recognized hydrodynamic software grounded in potential flow theory. The RAO reflects the buoy's response under a unit incident wave amplitude for a specific degree of freedom. Within the typical range where no significant nonlinearity occurs, the response (under a single frequency wave) can be evaluated by simply multiplying the actual wave amplitude by the RAO at the corresponding wave frequency. Since the integrated TENG's motion is driven by the buoy's movement, the buoy's hydrodynamic response provides valuable insights for the design of the R-TENG. Fig. 2a illustrates the setup of a single buoy, with a diameter of 0.26 m and a height of 0.7 m.

Fig. 2b-d present the RAO of the buoy with its center of gravity located 0.16 m above the keel. A linear viscous damping is applied in both the heave and pitch, with the damping ratio (evaluated empirically) set at 4.0 % of the critical damping. According to a survey [42], the effective wave heights in the northern Yellow Sea (e.g., nearshore, Dalian) typically do not exceed 1.2 m, and the mean wave period in this region generally ranges from 3 s to 5 s. Therefore, the wave period range in our analysis is set between 2 s and 6 s to capture the conditions outlined above.

With the increase of the wave period, the heave motion shows only slight variation, while the surge motion increases noticeably, and the pitch motion decreases markedly. Both the surge (translation) and pitch (rotation) motions can be harnessed to capture the wave energy. In designing the R-TENG, it is crucial to consider the primary working mechanism, i.e., whether designed in the translational or rotational mode, as well as the balance between the stability and internal load. In addition, the pitch angle under the actual sea conditions was evaluated based on typical wave heights (0.7 m to 1.2 m) and wave periods (3.8 s, 4.0 s, and 4.2 s) observed in the northern Yellow Sea. Based on the analysis, the pitch angle of the buoy is estimated at between 5°-12°.

2.3. Power generation assessment

To evaluate the energy harvesting performance of the R-TENG buoy array, a test platform was constructed, as shown in Fig. 3a. The setup consists of a controller, a 3 degree-of-freedom (3-DOF) motion platform, a desktop multimeter, and a signal monitor. Commands from the controller's master computer drive the 3-DOF platform to simulate the buoy's motion under wave excitations. The 3-DOF platform is actuated by three electric cylinders, enabling the production of multiple-DOF motions.

The motors were synchronized to produce the desired motion, thereby driving the R-TENG to generate electricity. The rectified outputs from the four-unit R-TENG array were measured, as shown in Fig. 3. It is worth noting that all the voltages/currents in this figure are the amplitude of the rectified (DC) output. θ represents the pitch of the buoy, and α represents the roll of the buoy. Fig. 3b presents the current outputs of the four units of R-TENG at a frequency of 0.5 Hz with a pitch angle of 10°, with all units connected in parallel. As shown in Fig. 3b (and Fig. S2), the current increases with the number of R-TENG units. This is because increasing the number of units can effectively improve the energy capture efficiency. It also can be seen the array configuration

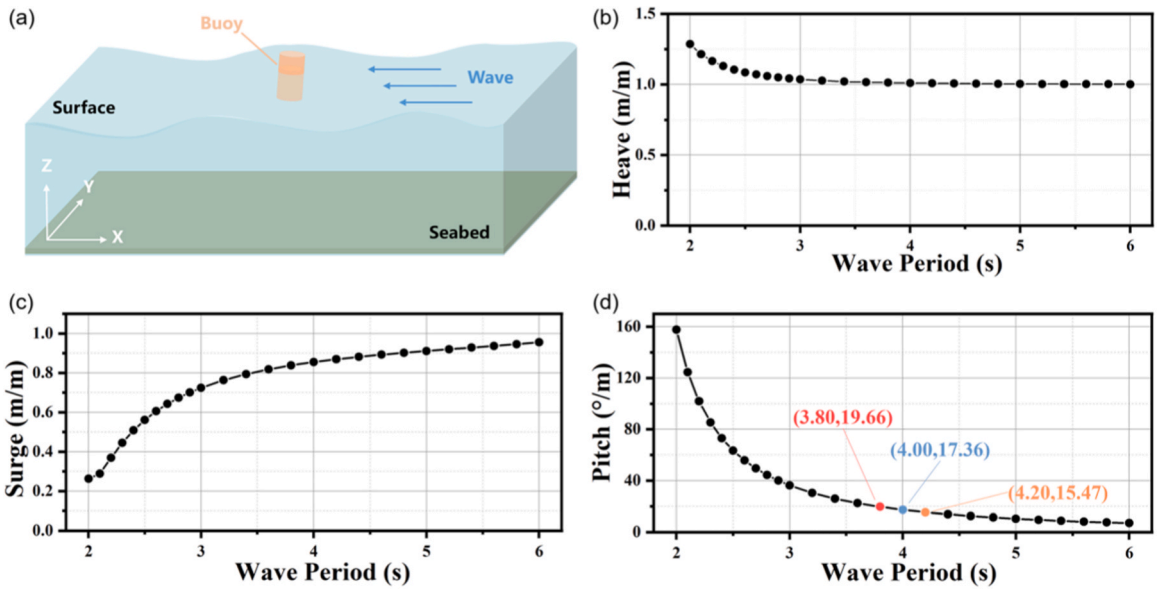

Fig. 2. Hydrodynamic analysis of the R-TENG buoy. (a) Schematic of a single buoy modeled in WAMIT. (b) Heave versus wave period, (c) Surge versus wave period, and (d) Pitch versus wave period.

can effectively enhance the energy harvesting performance.

In the rest of the subsection, the four TENG units housed in the buoy array were basically tested as a whole. Fig. 3c presents the voltage output of the four-unit R-TENG array at a frequency of 0.5 Hz under varying pitch angles, ranging from 4° to 12°. Experimental results show that as the pitch angle increases, the open-circuit voltage of the R-TENG array rises from 182.47 V to 954.36 V, and the short-circuit current increases from 34.89 μA to 411.91 μA. This should be attributed to the fact that a larger pitch angle allows the dielectric balls to roll over a longer distance, thus enhancing the triboelectric charging effect. The output of the R-TENG array was then further investigated by increasing the frequency from 0.2 Hz to 0.6 Hz at a fixed pitch angle of 10°. The results are plotted in Fig. 3d-e. As the frequency increased, the open-circuit voltage generated by the four-unit R-TENG array rose from 389.17 V to 1008.63 V, and the short-circuit current from 153.31 μA to 448.56 μA. This enhancement was attributed to the increased excitation frequency, which accelerated the dielectric balls and enhanced kinetic-to-electrical energy conversion.

In real sea conditions, the buoy experiences not only pitch motion but also small-angle rolling motion. Pitch (instead of roll) is the dominating effective motion for the device. To assess the influence of the small-angle rolling motion on the electrical output of the R-TENG array, tests were conducted under combined pitch and roll conditions. Fig. 3f-g present the electrical output at a frequency of 0.5 Hz, with roll angles of 2°, 3°, and 4°, and pitch angles of 6°, 8°, and 10°. The voltage/current output of the four-unit R-TENG array does not change significantly as the rolling angle increases, as the internal track in the R-TENG is aligned with the buoy's pitch motion. The current and voltage outputs at a pitch angle of 8° under varying rolling angles and frequencies are shown in Fig. 3 h and S3. It can be noted that the output of the R-TENG array rises with increasing frequency and remains relatively consistent across different rolling angles. Additionally, outputs at different rolling angles and frequencies for pitch angles of 6° and 10° are presented in Fig. S4. These results indicate that the output of the R-TENG array is primarily determined by the buoy's pitch angle and excitation frequency and is basically unaffected by small rolling angles.

2.4. Power modulation strategy

To further enhance the energy harvesting and charging performance of the R-TENG array, effective power modulation strategies (PMS) are indispensable. Fig. 4a shows the schematic diagram of the power modulation circuit designed to improve the performance of the R-TENG array. The system consists of an R-TENG array, a rectifier circuit, a power modulation circuit, and a load device. The four R-TENG units are connected in parallel, with each unit individually rectified to minimize energy loss and enhance charging efficiency. The PMS has a segmented topology. For most of the time, the storage capacitor at the input end is decoupled from the filter capacitor at the output end. Once the energy accumulated in the storage capacitor reaches a threshold, rapid switching allows the inductor to promptly transfer the stored energy to the output end. The filter capacitor helps stabilize the voltage output. This circuit regulates energy storage and release to ensure stable power delivery to the load. Fig. 4b compares the charging performance of a 6800 μF capacitor with and without PMS at a pitch angle of 10° and a frequency of 0.5 Hz. The results show a stepwise charging profile with a significantly higher charging rate when the PMS is applied. In addition, Fig. 4c demonstrates the charging behavior of a 10,000 μF capacitor at the same pitch angle of 10° but across different frequencies. Even at a low frequency of 0.1 Hz, the four-unit R-TENG array can charge a 10,000 μF capacitor to 5 V in 175 s.

Charging experiments were also carried out on electrolytic capacitors of 1000 μF, 2200 μF, 3300 μF, 4700 μF, 6800 μF, and 10,000 μF, as well as supercapacitors of 0.1 F, 0.22 F, and 0.47 F, at a pitch angle of 10° and a frequency of 0.5 Hz (as shown in Fig. 4d and S5). The results show that the four-unit R-TENG array enables fast charging of electrolytic capacitors and also exhibits good charging capability for supercapacitors.

An impedance matching test of the four-unit R-TENG array was performed, with the results shown in Fig. 4e. It can be found that the optimal matching resistance is about 5 MΩ, which corresponds to a peak power of 114.3 mW and a RMS power of 21.1 mW. To evaluate the durability of the R-TENG array in a real marine environment, an endurance experiment was conducted. Fig. 4f shows the output current of the four-unit R-TENG array over a continuous three-month period. While minor fluctuations are observed, the overall performance remains stable over time. Furthermore, scanning electron microscope (SEM) images of the PTFE balls, nylon balls, and copper foil were taken before (Fig. 4f(i)-(iii)) and after long-term operation (Fig. 4f(iv)-(vi)). The images show minimal surface wear, demonstrating the low-wear advantage of the orbital rolling design and confirming the durability of the R-TENG array.

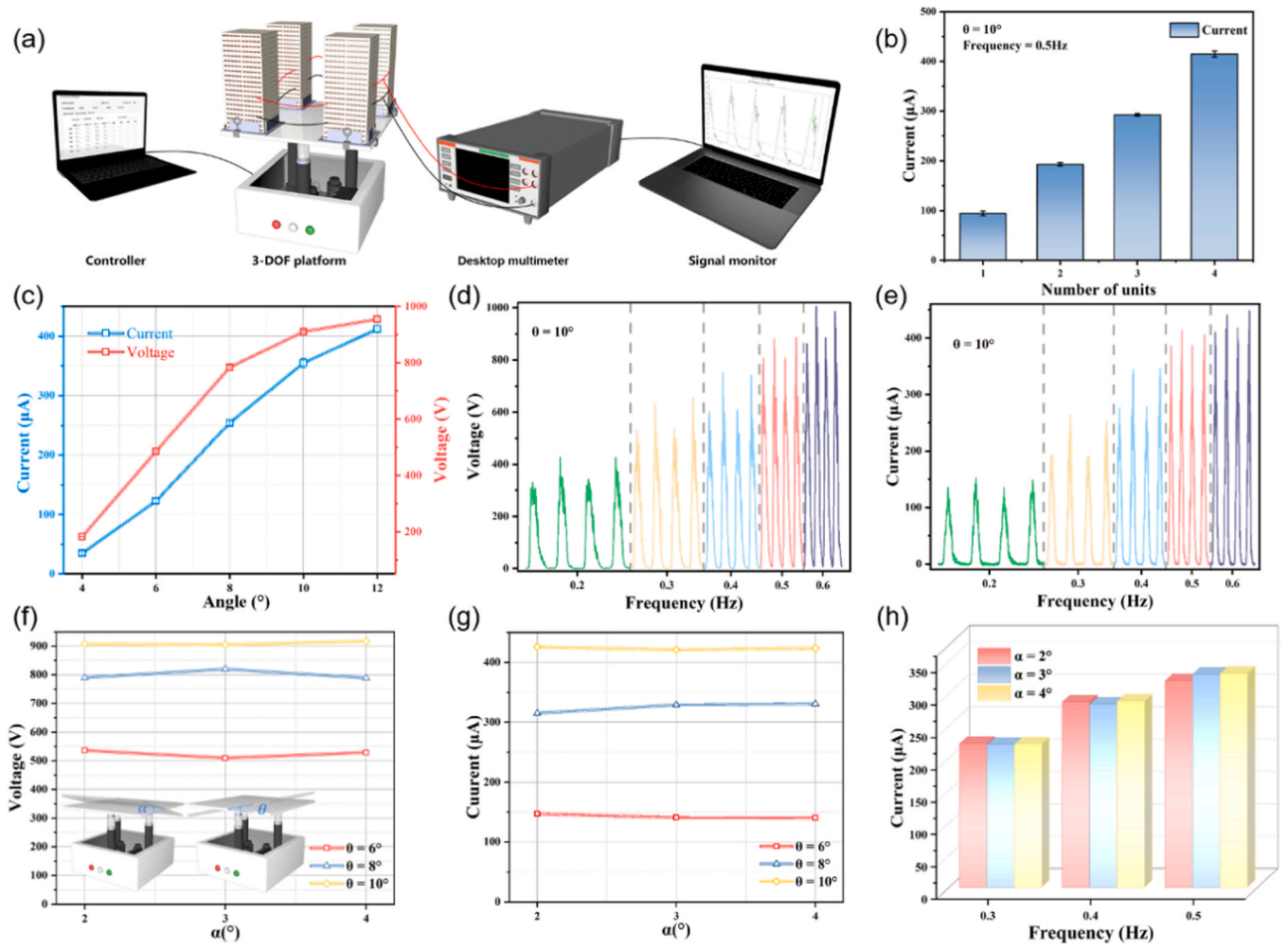

Fig. 3. Electrical performance of the four-unit R-TENG array. (a) Experimental setup for testing the R-TENG array. (b) Rectified output current with different numbers of R-TENG units. (c) Rectified voltage and current outputs at different pitch angles at a frequency of 0.5 Hz. (d) Rectified voltage and (e) current outputs of the R-TENG array at different frequencies with a constant pitch angle of 10°. (f, g) Rectified voltage and current of the R-TENG array outputs under varying roll angles (2°, 3°, 4°) at a frequency of 0.5 Hz and different pitch angles. (h) Influences of different frequencies and rolling angles on the rectified current output of the R-TENG array at a pitch angle of 8°.

2.5. *Application demonstration*

This subsection demonstrates the practical application of the R-TENG array. As shown in Fig. 5a and Supplementary Movie 1, the R-TENG array can light up 150 LED bulbs connected in series when driven by the 3-DOF platform operating at 0.5 Hz with a pitch angle of 10°. This examines the R-TENG array's potential to power navigational beacons in maritime environments.

Supplementary material related to this article can be found online at doi:10.1016/j.nanoen.2025.111318.

Fig. 5b presents the schematic of a wireless sensing system designed for integration with the buoy and powered by the R-TENG array. The R-TENG array charges a storage capacitor via the PMS, with energy managed by the LTC3588 module. The Undervoltage Lockout (UVLO) function of the LTC3588 module prevents the premature use of energy. Only when sufficient energy is accumulated, a low-power MCU (STM32) is activated, which then controls the sensors to measure temperature and pH levels. The monitored data is wirelessly transmitted via a LoRa module.

Fig. 5c and Supplementary Movie 2 demonstrate the measurement of water pH and wireless transmission, with the whole process solely powered by the R-TENG array in the laboratory environment. Supplementary Movie 2 shows that by switching the pH sensor between different water samples, the resulting changes in pH values confirm the sensor's proper functionality. Fig. 5d and Fig. S6 show the voltage variation on the capacitor (charged by the four-unit R-TENG array) during the sensing and wireless transmission process. Additionally, we repeated the test using a single R-TENG unit, with the results plotted in Fig. 5d. Compared with the four-unit R-TENG array, it is evident and not surprising that a single R-TENG takes significantly longer to activate monitoring and wireless transmission.

The above results indicate that the four R-TENG units can operate individually or cooperatively. Fig. 5e and Supplementary Movie 3 demonstrate the monitoring of temperature or pH data by each R-TENG unit (pH: N1, N2; Temperature: N3, N4). N1-N4 represent the four R-TENG units, respectively. To better demonstrate the transmission of pH and temperature information, the temperature sensor module is paired with an 8400μF capacitor, while the pH sensor module is paired with a 6800μF capacitor. In the forced motion experiments, successful wireless transmission of both water pH and temperature data was achieved, confirming that the R-TENG units can operate independently, thus enabling distributed monitoring of ocean data.

Supplementary material related to this article can be found online at doi:10.1016/j.nanoen.2025.111318.

A photograph of the buoy and the layout of the integrated wireless sensing and communication system is shown in Fig. 5f (the sensor in the

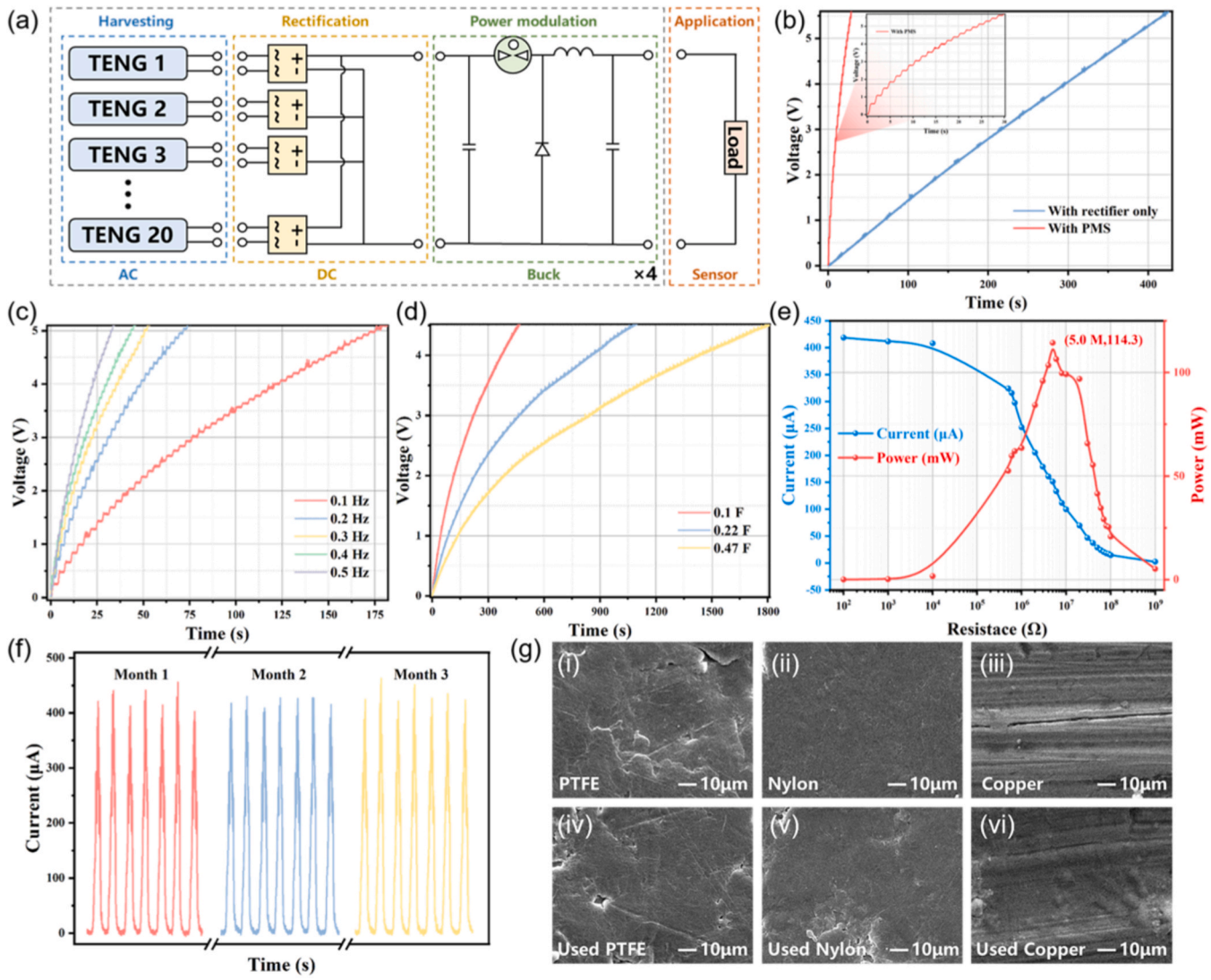

Fig. 4. Charging performance of the four-unit R-TENG array. (a) Schematic circuit diagram of the PMS. (b) Comparison of the capacitor (6800μF) charging speed for the R-TENG array with and without the PMS. (c) Charging behavior of a 10,000 μF capacitor by the R-TENG array under different frequencies at a pitch angle of 10°. (d) Charging performance of 0.1 F, 0.22 F, and 0.47 F supercapacitors using the R-TENG array with the PMS. (e) Output current and peak power of the R-TENG array as a function of load resistance, showing a peak power of 114.3 mW. (f) The endurance test result showing the current output of the R-TENG array over three consecutive months. (g) SEM images of PTFE balls, nylon balls, and copper foil before (i–iii) and after (iv–vi) long-term operation, illustrating material durability.

buoy designed is located outside the buoy, below the waterline). Each buoy was equipped with a single R-TENG unit operating independently. The buoy is tightly sealed between its upper and lower parts using sealing rings and anti-loosening screws. It also underwent water tightness testing in the laboratory water tank to ensure its sealing. To demonstrate the practical application of the R-TENG array, it was tested in a nearshore sea trial. Two buoys were used to monitor oceanic pH data (N1, N2), one buoy was used to monitor temperature (N4), and the fourth buoy (N3) was kept as a backup. During the sea trial, the wireless data transmission was basically stable. Fig. 5g illustrates the deployment of the R-TENG array and the onshore receiver during the sea trial. As shown in Fig. 5h and Supplementary Movie 4, the four-unit R-TENG array operated individually, successfully detecting in-situ temperature and pH level and transmitting the data to the onshore receiver (The wave conditions on the test day are shown in Table S1). These results validate that the R-TENG array exhibits applicable output performance in real marine environments and possesses distributed sensing capabilities for practical ocean monitoring applications.

Supplementary material related to this article can be found online at doi:10.1016/j.nanoen.2025.111318.

3. Conclusion

In this study, an innovative rolling-mode triboelectric nanogenerator (R-TENG) is developed to harness wave energy and provide an in-situ power solution for distributed marine sensing and monitoring applications. The proposed R-TENG leverages a ternary dielectric structure and a track-shell design to enhance charge transfer, reduce friction, and ensure stable operation under low-frequency, low-amplitude wave conditions. By arranging multiple R-TENG units in an array, the system significantly improves energy harvesting performance and spatial sensing coverage. Hydrodynamic simulations using WAMIT were conducted to predict the buoy's motion behavior, thereby ensuring alignment between wave excitation conditions and R-TENG's motion. Based on the frequency domain motion responses predicted by the hydrodynamic simulation, proper test conditions in the experiment were determined.

Experimental tests showed that the R-TENG array could easily power 150 LED bulbs, underscoring its practical energy output capability. Moreover, by adopting a power modulation strategy (PMS), the four-unit R-TENG array could charge a 10,000 μF capacitor to 5 V within

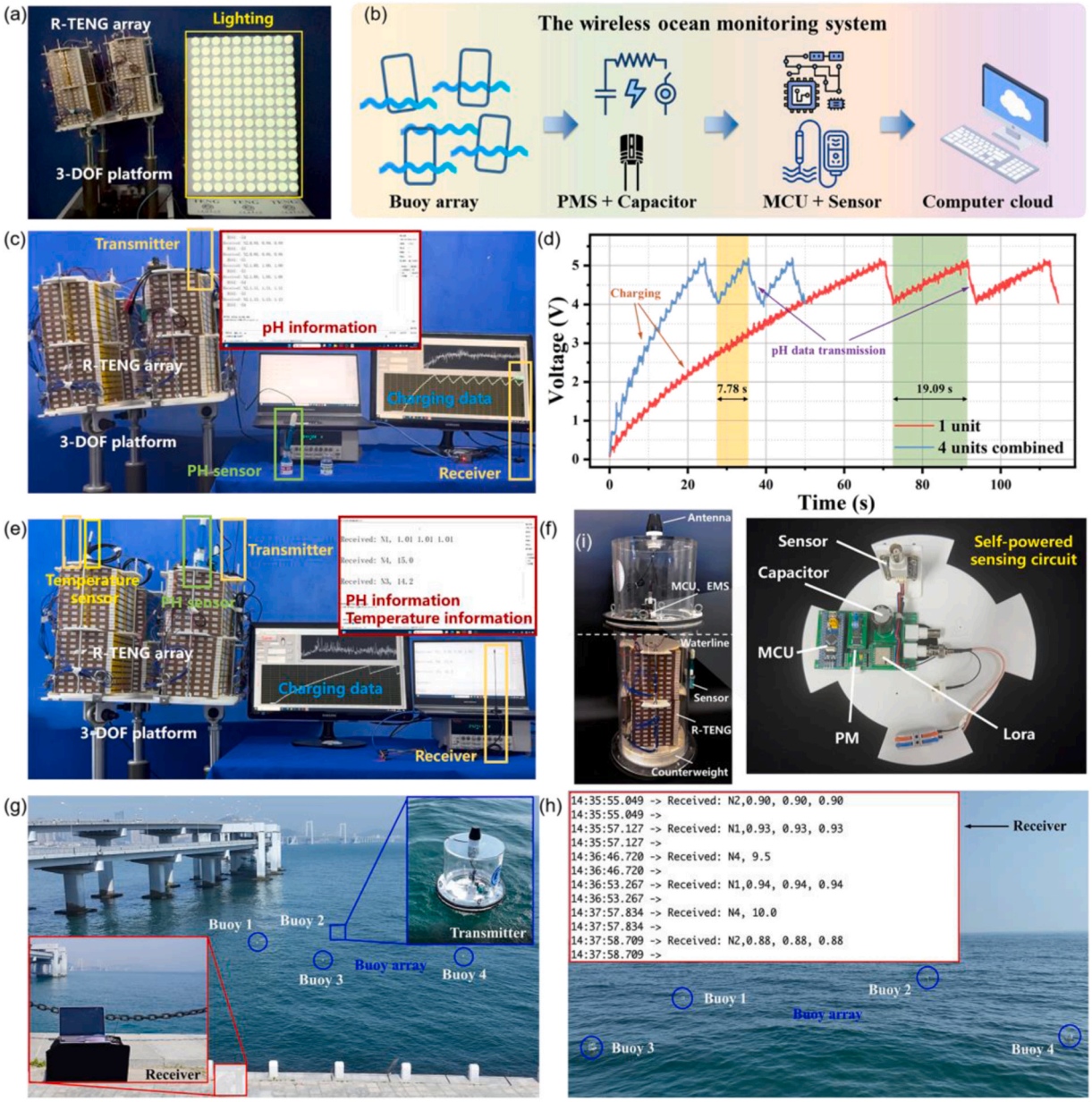

Fig. 5. Application demonstration of the R-TENG array. (a) Lighting up 150 LEDs using the four-unit R-TENG array. (b) Schematic of the wireless ocean monitoring system, comprising the buoy array, PMS, MCU, sensors, and cloud platform. (c) Demonstration of the self-powered pH sensing using the four-unit R-TENG array in the laboratory settings. (d) Voltage profiles across the capacitor during the self-powered pH sensing using a single R-TENG and the four-unit R-TENG array in the forced motion experiments. (e) Laboratory demonstration of self-powered sensing of both pH and temperature, with each R-TENG operating independently. (f) Photograph of the fabricated buoy prototype and the circuit module layout. (g) Nearshore sea trial of the R-TENG array for ocean data collection (each buoy carrying one R-TENG unit independently). (h) Real-time reception of pH and temperature data from each buoy at the onshore receiver.

175 s at a low frequency of 0.1 Hz. Furthermore, an optimal matching resistance of 5 MΩ was identified, corresponding to a peak output power of 114.3 mW. On top of these tests, a complete sensing and communication system was designed with low power requirements, enabling it to operate solely on the power supplied by the R-TENGs. By integrating the circuit board with a four-unit R-TENG array, autonomous wireless monitoring of pH and temperature is achieved. The functionality was validated in both forced experiments and real sea trials. During nearshore tests, each buoy (equipped with one R-TENG unit) independently sensed environmental data and transmitted it to an onshore receiver, confirming the feasibility of distributed sensing. Overall, the proposed R-TENG array presents a durable and scalable solution for self-powered ocean monitoring, representing a solid step forward in wave energy harvesting for practical applications. In the future, it can provide data support for offshore scenarios like offshore oil&gas, wind farms, marine ranching, oceanographic observation, and even defense applications.

4. Experimental methods

4.1. Fabrication of the R-TENG array

Each R-TENG unit consists of two PLA track shells, two PLA baffles, two sets of grating copper electrodes, three PTFE balls, and three nylon balls. First, the PLA track shell (157 mm long, 15.2 mm wide, containing 10 internal tracks with a 12.8 mm track diameter) and the PLA baffle (157 mm long, 16 mm wide) were designed using Solidworks and fabricated using a 3D printer (Bambu Lab P1S). Grating copper electrodes were then attached to the inner surfaces of both PLA shells.

Subsequently, PTFE balls (12.7 mm in diameter) and nylon balls (12.7 mm in diameter) were alternately placed in the tracks. The structure was covered with the second PLA shell and encapsulated with the PLA baffle. The final external fixation was completed using Kapton tape, resulting in a single R-TENG unit comprising twenty layers. In this study, four such R-TENG units, each embedded in an individual buoy, collectively form the R-TENG array.

4.2. Fabrication of the buoy

The acrylic buoy has a diameter of 0.26 cm, a top of 0.22 cm, a draft of 0.48 cm, and a total height of 0.7 m. The top and bottom parts of the buoy are sealed with rubber O-rings and secured with bolts. The bottom compartment houses the counterweight, the middle section holds the R-TENG units via an internal bracket, and the top part houses the circuit board, including the sensor module and the signal transmission module. A flange at the bottom allows for hanging the mooring weight, and a nylon rope is used as the mooring line.

4.3. Electrical measurements

The voltage and current outputs of the R-TENG array were measured using a benchtop multimeter (KEITHLEY DMM6500 6 1/2 DIGIT MULTIMETER). The charging characteristics were evaluated using a high-resistance electrometer (Keithley 6514). A three-degree-of-freedom platform (RWEC-3DOF-200-C-E-DP) was used to simulate wave excitations and evaluate the output performance of the R-TENG array.

4.4. Development of a wireless ocean sensing system

The wireless ocean monitoring system consists of a buoy array (each buoy carries an R-TENG unit), a rectifier bridge (DB107), a power modulation circuit (buck circuit), capacitors (6800 μF and 8400 μF), a microcontroller unit (STM32), a pH sensor (SEN0161-V2), a temperature sensor (DS18B20), a LoRa module (Ra-02) and a cloud platform. The pH sensor outputs an analog voltage, which is converted to a pH value using the formula: $pH = analogRead / 1024 \times 5000$ to get the actual pH value. The temperature sensor directly outputs the temperature reading directly as a digital output.

CRediT authorship contribution statement

Mingli Fan: Software, Validation, Visualization. **Shu Dai:** Supervision, Funding acquisition, Project administration. **Quanke Su:** Supervision, Resources. **Jingyi Liu:** Formal analysis, Visualization. **Hengxu Du:** Validation, Methodology, Investigation, Data curation. **Ziyue Xi:** Writing – original draft, Resources, Methodology, Investigation, Data curation. **Hongyong Yu:** Visualization, Methodology, Software. **Yawei Wang:** Methodology, Investigation, Data curation, Validation. **Hao Wang:** Writing – review & editing, Funding acquisition, Conceptualization, Supervision. **Minyi Xu:** Writing – review & editing, Funding acquisition, Conceptualization, Supervision. **Guobiao Hu:** Writing – review & editing, Funding acquisition, Methodology, Resources.

Declaration of Competing Interest

The authors declare that they have no known competing financial interests or personal relationships that could have appeared to influence the work reported in this paper.

Acknowledgements

Z. Xi, H. Du and Y. Wang contributed equally to this work. This work was supported by the National Key R&D Project from the Ministry of Science and Technology (Grant No. 2021YFA1201604), the National Natural Science Foundation of China (Grant No. 52471356, No. 52305135), the SIDRI Research Funding (Grant No. 2022QT(83)-035), the Fundamental Research Funds for the Central Universities (Grant No. 3132025214), and the Guangdong Provincial Project (Grant No. 2023QN10L545).

Appendix A. Supporting information

Supplementary data associated with this article can be found in the online version at doi:10.1016/j.nanoen.2025.111318.

Data availability

Data will be made available on request.

References

[1] F. He, Y. Liu, J. Pan, X. Ye, P. Jiao, Advanced ocean wave energy harvesting: current progress and future trends, J. Zhejiang Univ. Sci. A 24 (2023) 91–108, https://doi.org/10.1631/jzus.A2200598.
[2] L. Wang, J. Lin, H. Li, J. Jiang, S. Wu, G. Lu, Achieving efficient power generation for an enclosed drifting buoy by multi-DOF wave energy harvesting, Ocean Eng. 305 (2024) 117834, https://doi.org/10.1016/j.oceaneng.2024.117834.
[3] D. Yu, C. Sun, K. Wang, S. Yin, L. Sun, H. Chen, F. Kong, A novel direct-driven triboelectric–electromagnetic hybridized wave energy converter for buoy power supply, Appl. Nanosci. 12 (2022) 1697–1711, https://doi.org/10.1007/s13204-022-02398-6.
[4] J. Cui, H. Li, B. Chen, Z.L. Wang, A review of spherical triboelectric nanogenerators for harvesting high-entropy ocean wave energy, Chem. Eng. J. 499 (2024) 156193, https://doi.org/10.1016/j.cej.2024.156193.
[5] C. Zhang, Y. Hao, X. Lu, W. Su, H. Zhang, Z.L. Wang, X. Li, Advances in TENGs for marine energy harvesting and in situ electrochemistry, NanoMicro Lett. 17 (2025) 124, https://doi.org/10.1007/s40820-024-01640-w.
[6] C. Zhu, C. Xiang, M. Wu, C. Yu, S. Dai, Q. Sun, T. Zhou, H. Wang, M. Xu, Recent advances in wave-driven triboelectric nanogenerators: from manufacturing to applications, Int. J. Extrem. Manuf. 6 (2024) 062009, https://doi.org/10.1088/2631-7990/ad7b04.
[7] F. Jing, Y. Ni, S. Li, M. Shi, Dual-float-based triboelectric nanogenerator for low-frequency wave energy harvesting, Energy Tech. 12 (2024) 2301380, https://doi.org/10.1002/ente.202301380.
[8] C. Zhang, W. Yuan, B. Zhang, J. Yang, Y. Hu, L. He, X. Zhao, X. Li, Z.L. Wang, J. Wang, A Rotating Triboelectric Nanogenerator Driven by Bidirectional Swing for Water Wave Energy Harvesting, Small (2023), https://doi.org/10.1002/smll.202304412.
[9] Y. Ren, Z. Wang, J. Chen, F. Wu, H. Guo, An octave box inspired energy regularization triboelectric nanogenerator for highly efficient wave energy harvesting, Energy Environ. Sci. 17 (2024) 8829–8837, https://doi.org/10.1039/D4EE02969K.
[10] F. Wang, B. Cao, L. Shu, Z. Li, W. He, Z. Wang, P. Wang, High-performance triboelectric nanogenerator employing a swing-induced counter-rotating motion mechanism and a dual potential energy storage and release strategy for wave energy harvesting, Mater. Horiz. (2025), https://doi.org/10.1039/D4MH01491J.
[11] L. Liu, X. Yang, L. Zhao, H. Hong, H. Cui, J. Duan, Q. Yang, Q. Tang, Nodding duck structure multi-track directional freestanding triboelectric nanogenerator toward low-frequency ocean wave energy harvesting, ACS Nano 15 (2021) 9412–9421, https://doi.org/10.1021/acsnano.1c00345.
[12] M. Xu, T. Zhao, C. Wang, S.L. Zhang, Z. Li, X. Pan, Z.L. Wang, High power density tower-like triboelectric nanogenerator for harvesting arbitrary directional water wave energy, ACS Nano (2019), https://doi.org/10.1021/acsnano.8b08274.
[13] H. Wang, Z. Fan, T. Zhao, J. Dong, S. Wang, Y. Wang, X. Xiao, C. Liu, X. Pan, Y. Zhao, M. Xu, Sandwich-like triboelectric nanogenerators integrated self-powered buoy for navigation safety, Nano Energy 84 (2021) 105920, https://doi.org/10.1016/j.nanoen.2021.105920.
[14] W. Liu, L. Xu, T. Bu, H. Yang, G. Liu, W. Li, Y. Pang, C. Hu, C. Zhang, T. Cheng, Torus structured triboelectric nanogenerator array for water wave energy harvesting, Nano Energy 58 (2019) 499–507, https://doi.org/10.1016/j.nanoen.2019.01.088.
[15] C. Sun, X. Liu, W. Zhong, Q. Pan, L. Chen, G. Zhang, J. Wang, X. Dong, J. Shao, A kelp inspired high-power density triboelectric nanogenerator with stacking structure for multiple directional ocean wave energy harvesting, Adv. Mater. Technol. (2024) 2401183, https://doi.org/10.1002/admt.202401183.
[16] B. Yang, H. Li, Z. Wang, J. Wang, L. Dong, Y. Yu, J. Zhu, J. Zhu, T. Cheng, X. Cheng, High-performance triboelectric nanogenerator inspired by bionic jellyfish for wave energy harvesting, Chem. Eng. J. 503 (2025) 158399, https://doi.org/10.1016/j.cej.2024.158399.
[17] X.J. Zhao, H.L. Wang, Z.L. Wang, J. Wang, Nanocomposite electret layer improved long-term stable solid–liquid contact triboelectric nanogenerator for water wave energy harvesting, Small 20 (2024) 2310023, https://doi.org/10.1002/smll.202310023.
[18] Y. Nan, X. Wang, H. Xu, H. Zhou, Y. Sun, M. Wang, W. Liu, C. Ma, T. Yu, Submerged and completely open solid–liquid triboelectric nanogenerator for water

wave energy harvesting, InfoMat (2024) e12621, https://doi.org/10.1002/inf2.12621.
[19] D. Zhao, H. Li, J. Wang, Q. Gao, Y. Yu, J. Wen, Z.L. Wang, T. Cheng, A drawstring triboelectric nanogenerator with modular electrodes for harvesting wave energy, Nano Res. 16 (2023) 10931–10937, https://doi.org/10.1007/s12274-023-5796-6.
[20] H. Jung, Z. Lu, W. Hwang, B. Friedman, A. Copping, R. Branch, Z.D. Deng, Modeling and sea trial of a self-powered ocean buoy harvesting Arctic Ocean wave energy using a double-side cylindrical triboelectric nanogenerator, Nano Energy 135 (2025) 110641, https://doi.org/10.1016/j.nanoen.2024.110641.
[21] J. Yan, Z. Tang, N. Mei, D. Zhang, Y. Zhong, Y. Sheng, Triboelectric nanogenerators for efficient low-frequency ocean wave energy harvesting with swinging boat configuration, Micromachines 14 (2023) 748, https://doi.org/10.3390/mi14040748.
[22] P. Cheng, H. Guo, Z. Wen, C. Zhang, X. Yin, X. Li, D. Liu, W. Song, X. Sun, J. Wang, Z.L. Wang, Largely enhanced triboelectric nanogenerator for efficient harvesting of water wave energy by soft contacted structure, Nano Energy 57 (2019) 432–439, https://doi.org/10.1016/j.nanoen.2018.12.054.
[23] Y. Feng, X. Liang, J. An, T. Jiang, Z.L. Wang, Soft-contact cylindrical triboelectric-electromagnetic hybrid nanogenerator based on swing structure for ultra-low frequency water wave energy harvesting, Nano Energy 81 (2021) 105625, https://doi.org/10.1016/j.nanoen.2020.105625.
[24] J. He, X. Wang, Y. Nan, H. Zhou, Research progress of triboelectric nanogenerators for ocean wave energy harvesting, Small 21 (2025) 2411074, https://doi.org/10.1002/smll.202411074.
[25] H. Wang, J. Sun, Z. Xi, S. Dai, F. Xing, M. Xu, Recent progress on built-in wave energy converters: a review, JMSE 12 (2024) 1176, https://doi.org/10.3390/jmse12071176.
[26] H. Feng, C.X. Liu, W. Wang, Z. Dai, H. Zhang, H. Ma, Y. Yalikun, B. Zhang, C. Shang, Y.-C. Lai, Y. Yang, Omni-directional harvesting of ocean wave energy using arch-shaped double-layered direct-current triboelectric nanogenerator, Nano Energy 132 (2024) 110365, https://doi.org/10.1016/j.nanoen.2024.110365.
[27] Y. Xie, S. Wang, S. Niu, L. Lin, Q. Jing, J. Yang, Z. Wu, Z.L. Wang, Grating-structured freestanding triboelectric-layer nanogenerator for harvesting mechanical energy at 85% total conversion efficiency, Adv. Mater. 26 (2014) 6599–6607, https://doi.org/10.1002/adma.201402428.
[28] Y. Wang, H. Du, H. Yang, Z. Xi, C. Zhao, Z. Qian, X. Chuai, X. Peng, H. Yu, Y. Zhang, X. Li, G. Hu, H. Wang, M. Xu, A rolling-mode triboelectric nanogenerator with multi-tunnel grating electrodes and opposite-charge-enhancement for wave energy harvesting, Nat. Commun. 15 (2024) 6834, https://doi.org/10.1038/s41467-024-51245-5.
[29] M.G. Veurink, W.W. Weaver, R.D. Robinett, D.G. Wilson, R.C. Matthews, Efficient WEC array buoy placement optimization with multi-resonance control of the electrical power take-off for improved performance, OCEANS 2022 Hampton Roads (2022) 1–6, https://doi.org/10.1109/OCEANS47191.2022.9977067.
[30] E. Rainville, J. Thomson, M. Moulton, M. Derakhti, Measurements of nearshore ocean-surface kinematics through coherent arrays of free-drifting buoys, Earth Syst. Sci. Data 15 (2023) 5135–5151, https://doi.org/10.5194/essd-15-5135-2023.
[31] A. Fisher, J. Thomson, M. Schwendeman, Rapid deterministic wave prediction using a sparse array of buoys, Ocean Eng. 228 (2021) 108871, https://doi.org/10.1016/j.oceaneng.2021.108871.
[32] H. Wang, C. Zhu, W. Wang, R. Xu, P. Chen, T. Du, T. Xue, Z. Wang, M. Xu, A stackable triboelectric nanogenerator for wave-driven marine buoys, Nanomaterials 12 (2022) 594, https://doi.org/10.3390/nano12040594.
[33] Y. Wang, X. Liu, Y. Wang, H. Wang, H. Wang, S.L. Zhang, T. Zhao, M. Xu, Z. L. Wang, Flexible seaweed-like triboelectric nanogenerator as a wave energy harvester powering marine internet of things, ACS Nano 15 (2021) 15700–15709, https://doi.org/10.1021/acsnano.1c05127.
[34] Q. Zhang, M. He, X. Pan, D. Huang, H. Long, M. Jia, Z. Zhao, C. Zhang, M. Xu, S. Li, High performance liquid-solid tubular triboelectric nanogenerator for scavenging water wave energy, Nano Energy 103 (2022) 107810, https://doi.org/10.1016/j.nanoen.2022.107810.
[35] X. Liang, S. Liu, S. Lin, H. Yang, T. Jiang, Z.L. Wang, Liquid–solid triboelectric nanogenerator arrays based on dynamic electric-double-layer for harvesting water wave energy, Adv. Energy Mater. 13 (2023) 2300571, https://doi.org/10.1002/aenm.202300571.
[36] H. Liu, Y. Xiao, Y. Xu, S. Zhang, C. Qu, Y. Zhang, A highly adaptive real-time water wave sensing array for marine applications, Nanoscale 15 (2023) 9162–9170, https://doi.org/10.1039/D3NR00856H.
[37] R. Ouyang, Y. Huang, H. Ye, Z. Zhang, H. Xue, Copper particles-PTFE tube based triboelectric nanogenerator for wave energy harvesting, Nano Energy 102 (2022) 107749, https://doi.org/10.1016/j.nanoen.2022.107749.
[38] Y. Duan, H. Xu, S. Liu, P. Chen, X. Wang, L. Xu, T. Jiang, Z.L. Wang, Scalable rolling-structured triboelectric nanogenerator with high power density for water wave energy harvesting toward marine environmental monitoring, Nano Res. 16 (2023) 11646–11652, https://doi.org/10.1007/s12274-023-6035-x.
[39] Q. Li, W. Liu, H. Yang, W. He, L. Long, M. Wu, X. Zhang, Y. Xi, C. Hu, Z.L. Wang, Ultra-stability high-voltage triboelectric nanogenerator designed by ternary dielectric triboelectrification with partial soft-contact and non-contact mode, Nano Energy 90 (2021) 106585, https://doi.org/10.1016/j.nanoen.2021.106585.
[40] WAMIT USER MANUAL Version 7.4, Boylston St. USA (2022). https://www.wamit.com.
[41] Z. Wang, L. Lin, J. Chen, S. Niu, Y. Zi. Triboelectric Nanogenerator, First ed., 2017. Beijing, China.
[42] W. Qiu, G. Li, J. Xu, Y. Hu, Y. Wang, H. Shi, Spatial and temporal variation characteristics of the waves in the Yellow Sea and Bohai Sea, Mar. Sci. 45 (2021) 1–8, https://doi.org/10.11759/hykx20201109001.

Ziyue Xi is currently pursuing his doctor degree in Dalian Maritime University, china. His current research interests in the triboelectric nanogenerator, wave energy harvesting and self-powered systems.

Hengxu Du is pursuing a Ph.D. in Marine Engineering at Dalian Maritime University. His research focuses on nonlinear string vibration and structural health monitoring.

Yawei Wang is currently pursuing his doctoral degree at The Hong Kong University of Science and Technology (Guangzhou), China. His research focuses on vibration energy harvesting, self-powered systems, and battery-free marine observation systems.

Hongyong Yu is currently pursuing his doctor degree in Dalian Maritime University, china. His current research interests in the triboelectric nanogenerators and vibration energy harvesting.

Shu Dai received his PhD degree in ocean engineering from Texas A&M University. Currently, he is a senior engineer and research scientist in the Shanghai Investigation, Design and Research Institute Co., Ltd. His research interesting focus on the floating offshore wind turbine and random process in ocean environment conditions.

Mingli Fan is currently pursuing a master's degree at Dalian Maritime University in Dalian, China. His research focuses include wave energy collection, direct-drive electromagnetic generators, and self-powered ocean observation buoys.

Jingyi Liu is currently pursuing a master's degree at Dalian Maritime University in Dalian, China. His research focuses interests in the wave energy collection.

Quanke Su is the Chief Engineer and Professor of Practice at the Hong Kong University of Science and Technology (Guangzhou), with over 30 years of experience in transport infrastructure. From 2004–2022, he served as the Chief Engineer of the Hong Kong–Zhuhai–Macao Bridge, a world-class cross-harbor project. His research focuses on strategic planning and technical design of major engineering projects, structural durability for marine engineering, digital and intelligent construction, smart operation and maintenance, and integrated and autonomous transport systems.

Hao Wang received his PhD in ocean engineering from Texas A&M University. Currently, he is an associate professor in the Marine Engineering College of Dalian Maritime University. He has several years' engineering experiences in the offshore oil-&gas industry. His research focus on the wave energy conversion and hydrodynamics of ocean engineering.

Guobiao Hu is currently a tenure-track assistant professor with the IoT Thrust at HKUST(GZ). He received his Ph.D. degree from the University of Auckland, New Zealand. Before joining HKUST(GZ), he worked as a Research Fellow in the School of Civil and Environmental Engineering, at Nanyang Technological University. His research interests include energy harvesting technologies, battery-free Internet of Things, acoustic/elastic metamaterials, and intelligent material structures/systems.

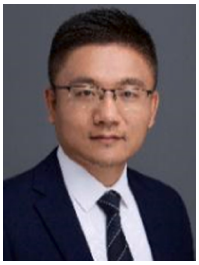

Minyi Xu received his Ph.D. degree from Peking University in 2012. During 2016–2017, he joined Professor Zhong Lin Wang' group at Georgia Institute of Technology. Now he is a Professor in the Marine Engineering College, Dalian Maritime University. His current research is mainly focused on the areas of blue energy, self-powered systems, triboelectric nanogenerators and its practical applications in smart ship and ocean.